Component Energy Efficiencies in a Novel Linear to Rotary Motion Inter-conversion Hydro-mechanism Running a Solar Tracker

Kant E. Kanyarusoke[*], Jasson Gryzagoridis, Modify Kaunda

Department of Mechanical Engineering, Cape Peninsula University of Technology, Cape Town, South Africa.

Abstract

A new mechanism interconverting linear and rotary motion was investigated for energy transfers among its components. It employed a gear-rack set, a Hooke coupling and a specially designed bladder-valve system that regulated the motion. The purpose was to estimate individual component mechanical efficiencies as they existed in the prototype so that future reengineering of the mechanism could be properly targeted. Theoretical modelling of the mechanism was first done to obtain equations for efficiencies of the key components. Two-stage experimentation followed when running a solar tracker. The first stage produced data for inputting into the model to determine the efficiencies' theoretical variation with the Hooke coupling shaft angle. The second one verified results of the Engineering Equation Solver (EES) software solutions of the model. It was found that the energy transfer to focus on was that between the Hooke coupling and the output shaft because its efficiency was below 4%.

Keywords: bladder, efficiency, gear-rack, Hooke coupling

1. Introduction

A new mechanism to interconvert linear and rotary motion had been designed. Kanyarusoke & Gryzagoridis [1] explain it as a weights driven, bladder-flow regulated mechanism that links linear motion of the weights to rotation of another mass about an axis inclined to the linear motion. Hooke and Waldron couplings are used to transfer energy between the two masses. In Kanyarusoke & Gryzagoridis [2], a prototype was tested in an application on solar tracking by a household photovoltaic (PV) panel. Jain [3] explains that the technical concern in systems of that size is whether the operation of the driving mechanism consumes a sizeable fraction of the extra energy it helps the panel generate. For example, results in [2] indicate that an average of about 4% of the gained energy was consumed over a 40 day period. On the worst tracking performance day, consumption was close to 27%. Clearly, there exists a need to investigate how this energy is expended. This work aims to do exactly that. Its novelty is that energy waste in each mechanical element is identified and quantified without dismantling the unit. Consequently, clear indications on where to focus reengineering effort in development of a commercial unit without separate testing of individual kinematic pairs are deduced.

Fig. 1 gives a broad view of the energy transfers in the mechanism. It would be the best if values of E_{resist} and E_f were zero. However, the second law of Thermodynamics precludes that possibility because we would then have a perpetual motion machine of the second order (Çengel, & Boles [4]). The energy E_f cannot be zero since the incompressible fluid must enter or exit the mechanism for the weights to move up or down. As for E_{resist}, it largely goes to overcome solid friction in the gear drive, in the Hooke coupling, in bearings, and it also overcomes fluid flow resistances. Even if friction and resistances were to be

---

* Corresponding author. E-mail address: kanyarusokek@cput.ac.za

Tel.: +27-21-9538741; cell: +27-78-4368347

insignificant, the Hooke joint always consumes energy because the component of the gear torque perpendicular to the rotating mass shaft does not contribute to energy transfer.
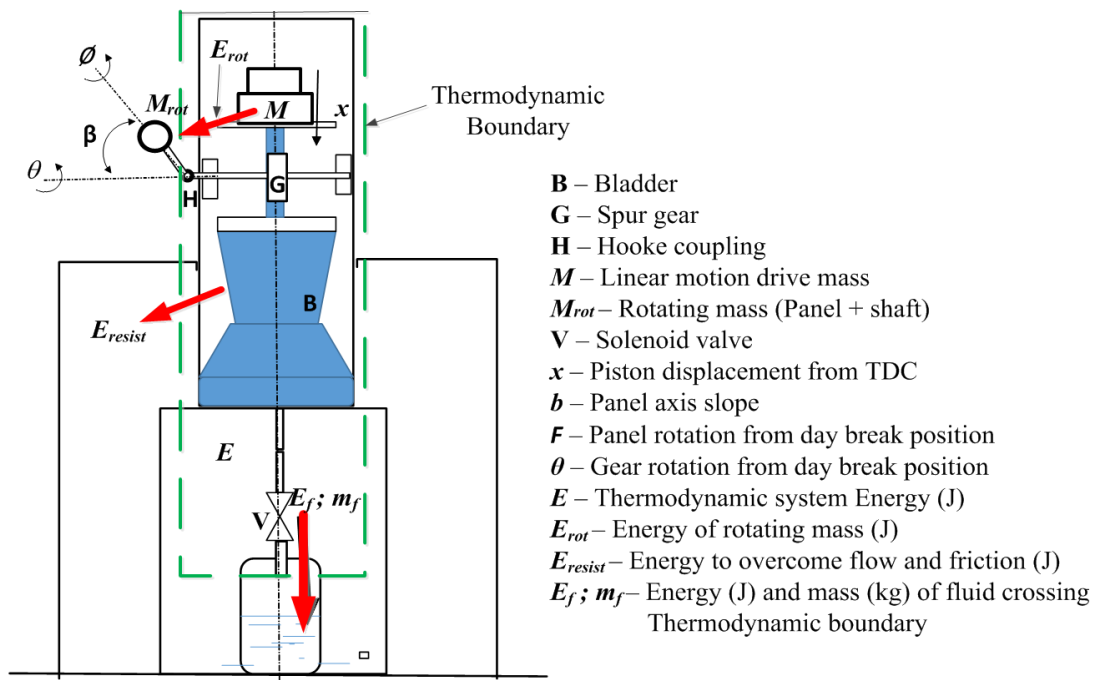

Fig. 1 Mechanism thermodynamics

B – Bladder
G – Spur gear
H – Hooke coupling
M – Linear motion drive mass
M_{rot} – Rotating mass (Panel + shaft)
V – Solenoid valve
x – Piston displacement from TDC
b – Panel axis slope
F – Panel rotation from day break position
θ – Gear rotation from day break position
E – Thermodynamic system Energy (J)
E_{rot} – Energy of rotating mass (J)
E_{resist} – Energy to overcome flow and friction (J)
E_f ; m_f – Energy (J) and mass (kg) of fluid crossing Thermodynamic boundary

Having figured out where the energy is expended within the mechanism, the issue was to try to quantify the various mechanical energy 'losses' so that future prioritized improvement could be targeted appropriately. Therefore, this paper first makes models of energy consumptions by individual components within the assembly. There is one problem, however: whereas the overall energy transfers to or from the linear motion mass are unidirectional during a motion-phase, those between the rotating mass and the Hooke coupling, sometimes reverse within the same phase because of rotation in a gravity field. The modelling is therefore done twice for each direction (up or down) of motion of the mass, *M*.

Experimentation follows modelling. Two sets of experiments are described. The first set determines the data to be input into the models' equations so that theoretical mechanical efficiencies of each key component can be determined. The second set verifies the computational results. The penultimate section of the paper discusses results of both sets. We conclude with a summary and a pointer to using the results in subsequent work.

2. Methodology

As pointed out above, the methodology adopted was: analytical modelling followed by experimentation. This is because the prototype was already in place. In modelling, the mechanics and hydraulics of the mechanism were examined in detail to derive equations of energy flows through each component for each of 4 stages in a complete up and down motion cycle of the mass *M*. The components are the gear-rack set; the Hooke coupling; the rotating shaft with its Waldron coupling, bearings and attached mass M_{rot} as a single unit; the hydraulic system – consisting of the in the feed pump (or whichever else source of head), the bladder and accompanying valves, piping and fittings. Because interest was in mechanical efficiency *η*, at each component the 1st law of Thermodynamics was used in the form of Eq. (1) to simplify the analysis.

$$E_{consumed} = (1-\eta) \sum_{all-in} E_{in} = \sum_{all-in} E_{in} - \sum_{all-out} E_{out} \tag{1}$$

In this section, we develop equations that eventually feed into Eq. (1) as a model in which efficiencies are to be solved for. The second part on methodology – which is experimentation – is described in section 4.

2.1. Essential kinematic equations of the Hooke joint

In Fig. 1, for a gear pitch diameter d_g, we have the linear relation:

$$\theta = \frac{2x}{d_g} \tag{2}$$

With the Hooke yokes in horizontal and vertical positions at the beginning of run, it is shown in standard Theory of Machines textbooks (e.g. Mabie &. Reinholtz [5], Kumar [6]) or even by vector analysis (Alugongo [7], Fischer & Paul [8]), that the input Hooke angle (in this case, θ) is related to the output angle ϕ by Eq. (3):

$$\theta = \tan^{-1}(\tan\varphi\cos\beta) \tag{3}$$

Differentiations yield Eqs. (4) and (5) for speeds.

$$\dot{x} = \frac{d_g}{2}\dot{\theta} \tag{4}$$

$$\dot{\theta} = \dot{\varphi}\cos\beta\frac{\cos^2\theta}{\cos^2\varphi} \tag{5}$$

2.2. Essential kinematic equation of the Bladder

For a bladder cone frustum of piston end diameter d_{piston}, (piston area A_{piston}) throat diameter d_{throat} and frustum height h_{cone}, geometry and incompressible fluid continuity yield Eq. (6) for the flow rate, $\dot{V}$:

$$\dot{V} = \frac{dV}{dx}\dot{x} = (1 - \frac{x}{h_{cone}}(1 - \frac{d_{throat}}{d_{piston}}))^2 A_{piston}\dot{x} \tag{6}$$

Eq. (6) makes two important assumptions:

(1) The bladder is so constrained by its covering as not to distend on pressurization. In design and construction, this was approximated first by using a much stiffer material for the covering and secondly by making the bladder and covering 'as-made' dimensions very nearly equal.

(2) On emptying of the frustum, although the piston is always in contact with the fluid, there is no fluid hold up in the resulting folds. This can only be approximated by ensuring perfect bladder symmetry about the line of motion of the driving weights' center of gravity. In the design, attempts to achieve this were by placing the weights centrally and providing four 90° centrally positioned rolling element bearings to guide the piston rod.

2.3. Essential energy transfer equations

For energy transfer from the gear set, through the Hooke coupling to the rotating mass, if the efficiencies are denoted as η_g, η_H and η_s respectively, Fig. 2 shows the gear torque distribution. Eqs. (7) and (8) give the torque and Hooke coupling efficiency (the latter ignores effects of internal coupling friction) relationships.

$$T_s = \eta_g\frac{F_t d_g}{2}\cos\beta \tag{7}$$

$$\eta_H = \frac{T_s\dot{\varphi}}{\eta_g T_g\dot{\theta}} = \frac{\dot{\varphi}\cos\beta}{\dot{\theta}} = \frac{\cos^2\varphi}{\cos^2\theta} = \cos^2\varphi + \sin^2\varphi\cos^2\beta \tag{8}$$
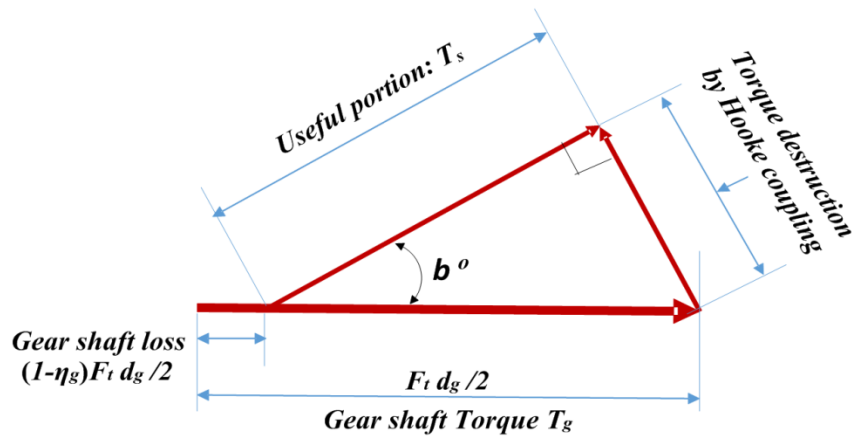
Fig. 2 The gear torque split diagram

2.4. *Fluid flow out of the bladder*

Referring to Fig. 3: if the solenoid valve is open and the piston pressure is *P*, we can write:

$$P = \frac{\rho_f C^2}{2}[(1+K_l) - \frac{C_{piston}^2}{C^2}] - \rho_f g\ (h_0 - x) \qquad (9)$$

where C_{piston} is the piston retraction speed (or *dx/dt*); *C* is the discharge fluid velocity; K_l is a mechanical energy loss coefficient arising out of: entry into discharge pipe (1.0), friction in pipe and flow through the fully open valve (0.25).
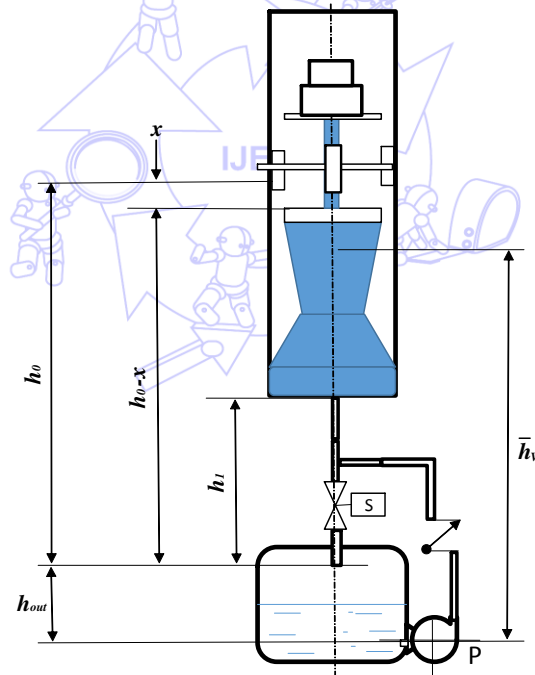

Fig. 3 Fluid flow system

With bracketed values of coefficients from Çengel, & Cimbala [9] and Douglas et al. [10], the coefficient K_l is seen to be:

$$K_l = 1.25 + \frac{4h_1 f}{d_{pipe}} \qquad (10)$$

The Darcy friction factor *f* depends on the nature of flow. Experimentation with the prototype - such as described later in section 4 - showed that depending on the magnitudes of driving forces and ambient conditions, the flow can be either laminar or turbulent. Therefore, Eqs. 11(a) and 11(b) from [9] and [10] can be used for laminar and turbulent flow in a smooth plastic pipe employed in the prototype.

$$f = \frac{16}{\text{Re}} = \frac{4\pi\mu_f d_{pipe}}{\rho_f \dot{V}_f} \qquad\qquad (Laminar\ flow) \qquad\qquad (11a)$$

$$f = \frac{0.079}{\text{Re}^{0.25}} = 0.079(\frac{\pi\mu_f d_{pipe}}{4\rho_f \dot{V}_f})^{0.25} \qquad\qquad (Turbulent\ flow) \qquad\qquad (11b)$$

On substitution in Eqs. (9) and (10), ignoring the speed ratio square $(C_{piston}/C)^2$ and subsequent simplifications, for specific system design, either of Eqs. (12a) and (12b) results:

$$P = P_0 + p_x x + p_{v1}\dot{V} + p_{v2}\dot{V}^2 \qquad\qquad (Laminar\ flow) \qquad\qquad (12a)$$

$$P = P_0 + p_x x + p_{vt}\dot{V}^{1.75} + p_{v2}\dot{V}^2 \qquad\qquad (Turbulent\ flow) \qquad\qquad (12b)$$

where P_0, p_x, p_{vt}, p_{v1} and p_{v2} are system design constants defined by Eq. (13).

$$P_0 = -\rho_f g h_0 \qquad\qquad (13a)$$

$$p_x = \rho_f g \qquad\qquad (13b)$$

$$p_{v1} = \frac{128\mu_f h_1}{\pi d_{pipe}^4} \qquad\qquad (13c)$$

$$p_{vt} = 0.241 h_1 \sqrt[4]{\frac{\mu_f \rho_f^3}{d_{pipe}^{19}}} \qquad\qquad (13d)$$

$$p_{v2} = \frac{20\rho_f}{\pi^2 d_{pipe}^4} \qquad\qquad (13e)$$

3. Modelling for experimentation

Detailed energy transfers in the mechanism depend on whether the bladder is filling up or is being emptied: and in each of these two cases, whether the angle $\emptyset$ is less or greater than 90°. In this section, for all the four situations, we use the concept of mechanical efficiency and trace the transfers between mechanism components and to/from outside. From this, we derive two equations for gear and shaft efficiencies. These equations will have to be solved later in order to determine how the efficiencies vary with the Hooke shaft angle b.

3.1. Fluid flow into the bladder

Prior to operation, the mechanism is energized by a suitable hydraulic head source (e.g. pump or feed from a raised fluid reservoir) such that the drive masses have an energy ΔE_M and the fluid has energy $\Delta E_{f\text{-}in}$ relative to the 'dead' state at a position defined by $\emptyset = 180°$. Energy is transferred to the drive masses in two stages: when $\emptyset > 90°$ and when $\emptyset < 90°$. In the former, energy from the hydraulic system is shared between the masses and the rotating mass. The masses are lifted to the mid position and gain potential energy $0.5\Delta E_M$. In the second phase, they receive the balance $0.5\Delta E_M$ from both the hydraulic system and the rotating mass because of gravity effects on rotation. Recalling that efficiency is simply a ratio of 'useful energy' transferred out of a mechanical element to the total input energy, we can then model the energy flows during bladder fill-up as in Fig. 4.

During the period when $\emptyset > 90°$, at the output shaft we have:

$$M_{rot} g e \cos\beta = \eta_s \eta_H E_{H\text{-}in} \Rightarrow E_{H\text{-}in} = \frac{M_{rot} g e \cos\beta}{\eta_s \eta_H} \qquad\qquad (14)$$

Hence for the gear rack set we can write:

$$E_{g-in1} = \frac{1}{\eta_g}[0.5\Delta E_m + \frac{M_{rot}ge\cos\beta}{\eta_s\eta_H}] \tag{15a}$$

And when $\emptyset < 90°$,

$$E_{g-in2} = \frac{0.5\Delta E_m}{\eta_g} - \eta_s\eta_H M_{rot}ge\cos\beta \tag{15b}$$

Then:

$$E_{g-in} = E_{g-in1} + E_{g-in2} = \eta_p E_{in} - \Delta E_{f-in} - E_{r-f-in} \tag{15c}$$

Balancing energy in the hydraulic system for the entire duration of inflow:

$$\eta_p E_{in} - \Delta E_{f-in} - E_{r-f-in} = \frac{\Delta E_m}{\eta_g} + M_{rot}ge\cos\beta(\frac{1}{\eta_g\eta_s\eta_H} - \eta_s\eta_H) \tag{16}$$
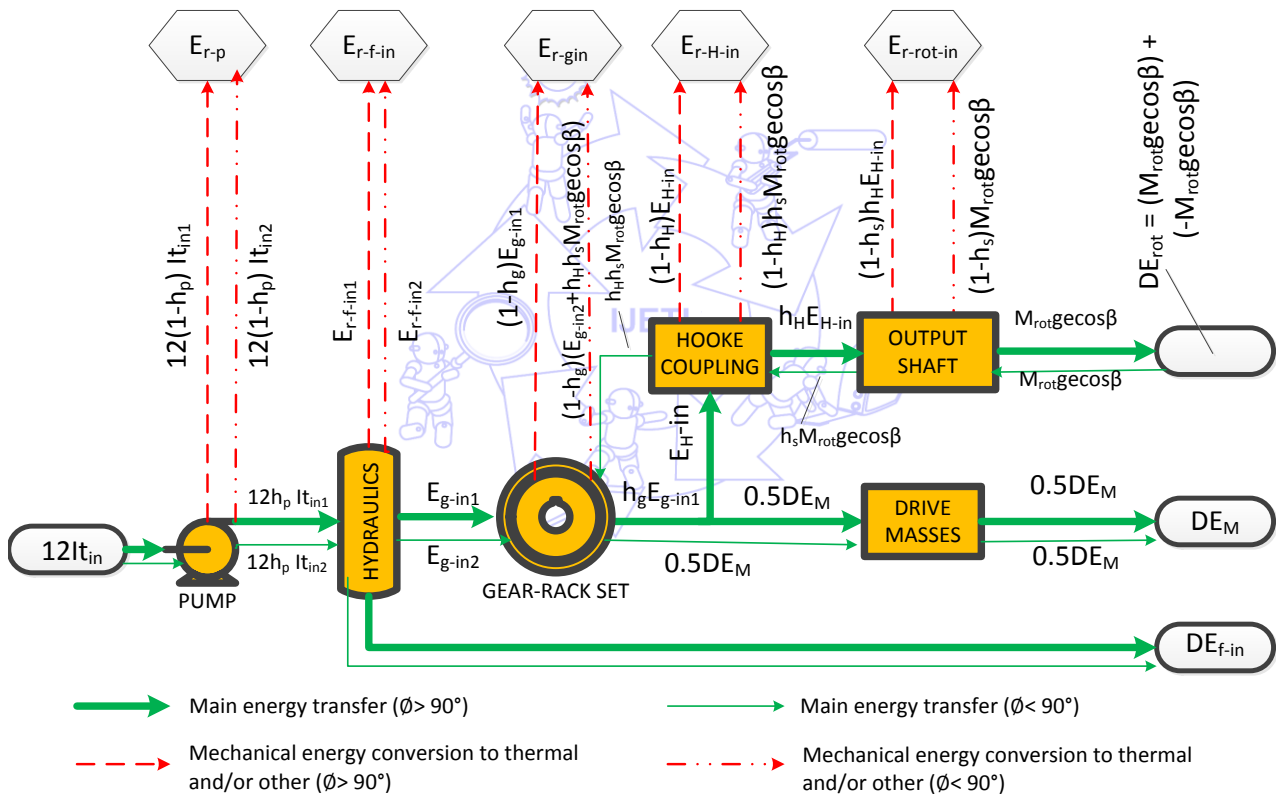

Fig. 4 Energy transfers in the new hydro-mechanism during bladder inflow

3.2. Fluid outflow from the bladder

During the bladder outflow, the drive masses descend. Considerations similar to those in section 3.1 lead to energy transfers depicted in Fig. 5. Considering energy into and out of the gear rack set, we have:

For $\emptyset < 90°$:

$$E_{g-out1} = 0.5\eta_g\Delta E_m - E_H = 0.5\eta_g\Delta E_m - \frac{M_{rot}ge\cos\beta}{\eta_s\eta_H} \tag{17a}$$

For $\emptyset > 90°$:

$$E_{g-out2} = \eta_g[0.5\Delta E_m + \eta_H\eta_s M_{rot}ge\cos\beta] \tag{17b}$$

Totaling the two for the entire outflow period gives:

$$E_{g-out} = \eta_g \Delta E_m - M_{rot} g e \cos\beta (\frac{1}{\eta_s \eta_H} - \eta_g \eta_s \eta_H) \tag{17c}$$

And hence for the hydraulic system we have:

$$\eta_g \Delta E_m - M_{rot} g e \cos\beta (\frac{1}{\eta_s \eta_H} - \eta_g \eta_s \eta_H) = \Delta E_{f-out} + E_{r-f-out} - \Delta E_{f-in} \tag{18}$$

The problem addressed in this paper is to solve Eqs. (16) and (18) simultaneously for η_g and η_s at each of the angles β (which therefore defines the Hooke coupling efficiency η_H).
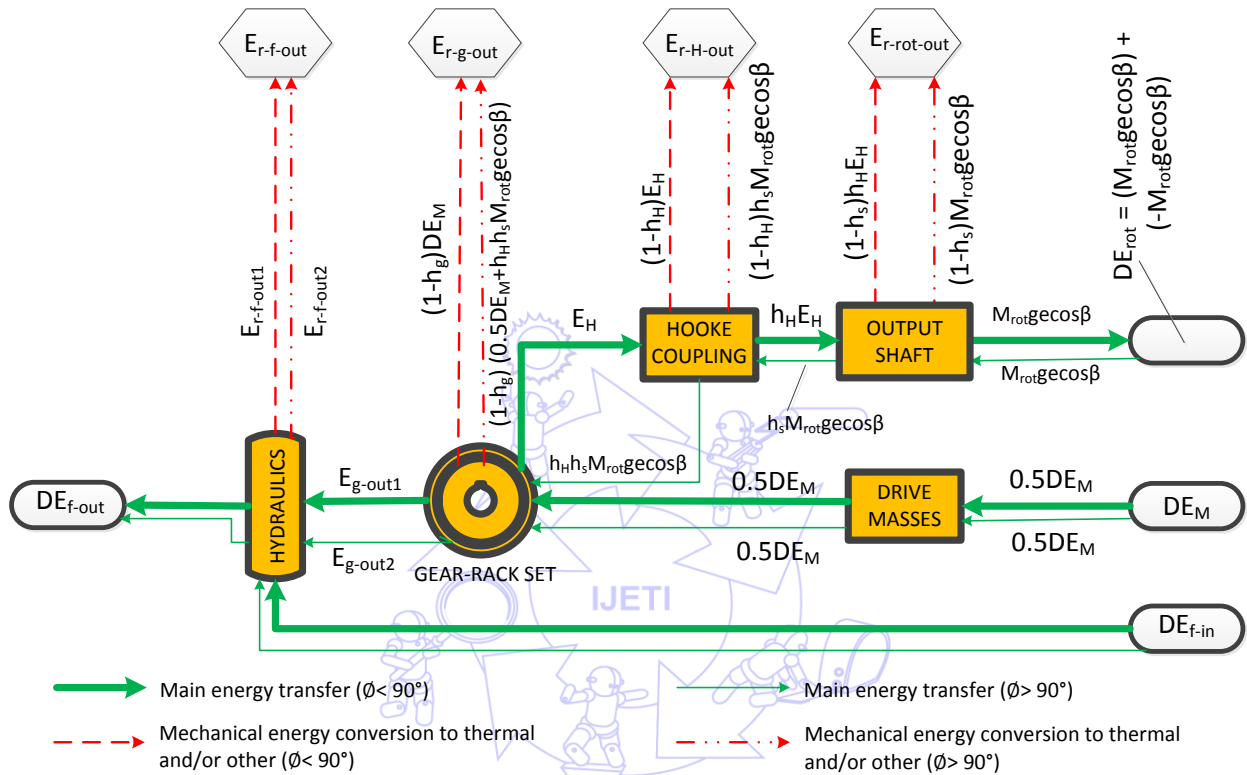

Fig. 5 Energy transfers in the new hydro-mechanism during bladder outflow

3.3. Solving the equations

Solving Eqs. (16) and (18) for η_g and η_s requires two types of data. The first type is the physical data of the experimental rig or prototype. Section 3.3.2 gives this data. The second type is experimental data from which the energy quantities ΔE_m, ΔE_{f-out}, ΔE_{f-in}, ΔE_{r-f-in}, $\Delta E_{r-f-out}$ and $\eta_p E_{in}$ can be determined. This is given later in section 4. But to use it, equations relating it to these energy terms are required. Also to simplify the analysis, a suitable average value of the Hooke coupling efficiency η_{H-av} is determined for continuous rotation between two positions $\emptyset_1$ and $\emptyset_2$. Hence, in the next subsection, we give their summary.

3.3.1. The Energy terms ΔE_m, ΔE_{f-out}, ΔE_{f-in}, ΔE_{r-f-in}, $\Delta E_{r-f-out}$ and $\eta_p E_p$

Let V be the volume pumped into the bladder in a time t_{in}, lifting the piston from Bottom Dead Centre (BDC) to Top Dead Centre (TDC), and then discharged out in time t_{out}, returning the mechanism to its initial thermodynamic state. Then, for turbulent flow in the inlet/discharge pipe, the energy terms can be computed from Eq. (19). This set of equations has approximated the flow rates to constant values, V/t_{in} and V/t_{out} for simplicity. It is derived from considerations of overall energy changes between piston BDC and TDC of: reciprocating masses (19a), pressurised static fluid in full bladder (19b), out flow fluid (19e), in and out flow mechanical energy losses (19c and 19d), and finally, supply pump energy (19f).

$$\Delta E_M = (M + M_{piston}) g x_{max} \tag{19a}$$

$$\Delta E_{f-in} = (P_{static} + \rho_f g \bar{y}_b) V_b + \rho_f g V (\bar{y}_{b-low} + x_{max} - \bar{y}_V) - \rho_f g \bar{y}_{b-low} (V_b - V)$$
$$= (P_{static} + \rho_f g \bar{y}_b) V_b + \rho_f g [V(x_{max} - \bar{y}_V) - (V_b - 2V)\bar{y}_{b-low}][V(x_{max} - \bar{y}_V) - (V_b - 2V)\bar{y}_{b-low}] \tag{19b}$$

$$E_{r-f-in} = [5.7 + \frac{0.2082}{d_{pipe}} (\frac{\mu_f d_{pipe} t_{in}}{\rho_f V})^{0.25}] \frac{\rho_f V^3}{2 t_{in}{}^2 A_{pipe}{}^2} \tag{19c}$$

$$E_{r-f-out} = [1.25 + \frac{0.1190}{d_{pipe}} (\frac{\mu_f d_{pipe} t_{out}}{\rho_f V})^{0.25}] \frac{\rho_f V^3}{2 t_{out}{}^2 A_{pipe}{}^2} \tag{19d}$$

$$\Delta E_{f-out} = \frac{\rho_f V^3}{2 A_{pipe}{}^2 t_{out}{}^2} + \rho_f V g h_{out} \tag{19e}$$

$$\eta_p E_{in} = \rho_f g H_{pump} V \tag{19f}$$

$$\eta_{H-av} = \eta_{H\varphi_1,\varphi_2} = \frac{1}{\varphi_2 - \varphi_1} \int_{\varphi_1}^{\varphi_2} \eta_H d\varphi = \frac{1 + \cos^2 \beta}{2} + \sin^2 \beta [\frac{\sin 2\varphi_2 - \sin 2\varphi_1}{4(\varphi_2 - \varphi_1)}] \tag{20a}$$

where H_{pump} is peak pump head developed during delivery of fluid volume V into bladder (m), P_{static} is pressure at piston when at rest (e.g. at TDC with all valves closed) (Pa), V_b is total volume of full bladder (m³), $\bar{y}_b$ is distance of centroid of fluid volume from piston when at TDC (m), $\bar{y}_{b-low}$ is distance of centroid of fluid remaining in bladder from piston when at BDC (m), and $\bar{y}_V$ is distance of centroid of added fluid V from piston when at TDC (m). Use of this equation is subject to the conditions:

$$n\frac{\pi}{4} \leq \varphi_1 < \varphi_2 \leq (n+1)\frac{\pi}{4}, \text{ for } n = 0, 1, 2, 3 \tag{20b}$$

3.3.2 .Experimental rig (Prototype) data

The apparatus was designed to enable $180°$ rotation for a piston displacement of 141.2 mm at a variable Hooke coupling shaft angle between 0 and 30°. Table 1 gives its data.

Table 1 Experimental rig data

Rotating mass M_{rot} (kg)	11.400	Piston – rack – rod mass M_p (kg)	2.500
Radius of gyration k_{rot} (m)	0.137	Piston diameter d_{piston} (m)	0.160
Eccentricity e (m)	0.0136	Maximum piston displacement x_{max} (m)	0.141
Hooke coupling shaft angle b (Rad)	Controlled	Bladder throat diameter d_{throat} (m)	0.127
Rotation transmission efficiency η_s	Stochastic: Experimental	Bladder emptying part height h_{cone} (m)	0.150
Gear module m (m)	0.003	Working fluid	Water
Gear teeth z	30	Fluid density ρ (kg/m³)	998.2
Gear pitch diameter d_{gear} (m)	0.09	Fluid viscosity μ (Pa.s)	0.00102
Gear drive efficiency η_g	Experimental	Discharge pipe internal diameter d_{pipe} (m)	0.0152
Max. piston height above valve h_0 (m)	0.750	Valve minimum pressure drop P_{v-min} (Pa)	10 000
Discharge pipe length h_1 (m)	0.400	Driving masses	Controlled

The pump manufacturer gives data on the pump characteristic. The fourth order polynomial curve fit for the data is given by Eq. (21).

$$H(m) = 4 - 0.21\dot{V}(l/\min) - 0.0073\dot{V}^2 + 0.012\dot{V}^3 - 0.001\dot{V}^4 \tag{21}$$

This completes the modelling. Next, we describe the experiments.

4. Experimentation

Many experiments with driving masses between 3 and 9 kg - and at angle b values of 0 to 30° - were done in the period 4th July-14th Nov 2015. However, the focus here is on one set that used the 9 kg mass. Here, we report the part that helped us estimate the mechanism's efficiencies η_s and η_g in a real working environment (outdoors).

4.1. Tools and equipment

(1) The designed rig (as in Table 1) with its loaded output shaft at a variable slope b°.

(2) Standard commercial weights: 1 kg: 1 off; 2 kg: 4 off.

(3) Measuring cylinder: Capacity 1000 ml. Graduations: Main 100 ml. Minor 10 ml.

(4) Stop watch: Sports grade - reading to 0.01 s.

(5) Video camera to supplement the stop watch in timing: Samsung HMX-F90 HD Recorder 1280X720

(6) Low pressure gauge: 0-250 mbar with 5 mbar graduations. Max. Error = 1% full scale reading (2.5 mbar). Manufacturer: Cape Instruments – South Africa.

(7) Measuring tape – Graduation: mm.

(8) Weather station – (for wind speed and ambient temperature): Campbell Scientific equipment logging 15 minute data

(9) Smart phone: Black Berry Z 10 with 'Protractor' application loaded (for set up of angles – but cross checked by Trigonometric computations).
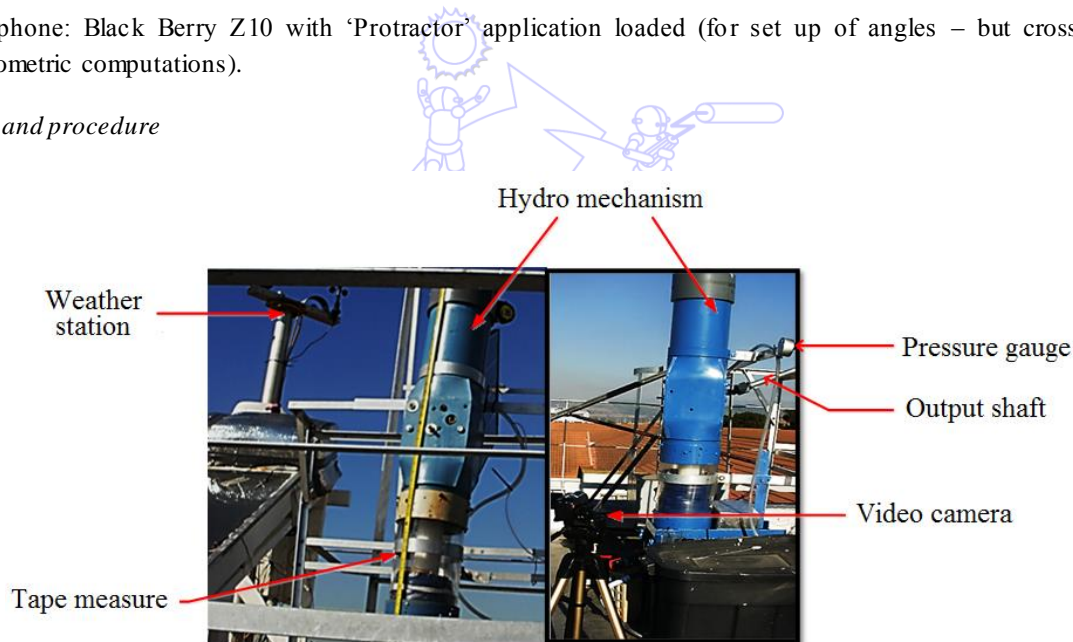
4.2. Setup and procedure

Fig. 6 Experimental setup

The rig was set up as in Fig. 6. For each angle, a paper template was made to match piston advance from (TDC) with rotation angle Ø at key steps. Eqs. (2) and (3) facilitated this. Both the tape measure and template were affixed to the mechanism transparent housing such that the template zero mark had minimal parallax with the top edge of the bladder when at TDC. It is motion of this edge that was to be monitored during the experiments.

At each controlled variable Hooke angle b, water was pumped into the mechanism so that the piston moved from BDC to TDC - by which time the rotating mass had turned through 180° in one direction. The time for this travel was recorded as t_{in} using both the video camera and the stop watch. The piston gauge pressure, P_{static} at TDC was recorded.

Immediately after these recordings, the solenoid valve at the bottom of the mechanism was energized to discharge the fluid so that the rotating mass turned in the reverse direction. The reversal time t_{out} was recorded, and so was the volume V - discharged, between TDC and BDC. At BDC, the gauge pressure, P_{static} was virtually zero. Ambient conditions of temperature and wind speed were noted from the adjacent weather station (fully described in Kanyarusoke, et al. [11]).

For each b ° value (0, 5, 10, 15, 20, 25, 30), this procedure was done 15 times on different occasions within the test period. This was intended to capture as wide a range of environmental conditions as possible (winter to towards summer) so that a fairly representative appreciation of efficiencies could be made. Another purpose for the repetitions was the minimization of effects of experimental errors on the overall results. Out of a possible total of 105 result sets, 2 were incomplete because experiments were stopped midway on account of rain. Three others were discarded because they could not yield solvable equations by the EES software – most likely because of errors in the readings. Another was discarded as a statistical 'outlier', well isolated from the rest in the group of experiments for the particular Hooke angle. This left 99 sets or 94.3% of target for use in the analysis.

4.3. Primary data – sample results

Four pieces of data were recorded for each result set: Peak piston pressure P_{static} (represented by P in Table 2) on filling the bladder (which was controlled at 4 kPa); in-flow and out-flow times tin, tout and discharge volume V (which was assumed to be equal to the inflow volume). Sample results are given in Table 2.

Table 2 Sample primary data for 4 July to 14 Nov 2015

$\beta = 0°$: 4th July to 14 Nov 2015

PRIMARY DATA (Measured)			
P (kPa)	t_{in} (s)	t_{out} (s)	V (L)
4	54.3	30.3	3.00
4	54.8	32.4	3.10
4	52.1	35.3	3.10
4	52.3	34.6	3.00
4	53.1	32.9	3.00
4	52.5	46.6	3.10
4	51.9	46.6	3.20
4	53.5	48.9	3.10
4	53.1	54.0	3.10
4	52.3	49.7	3.10
4	53.8	40.9	3.10
4	53.5	46.2	3.10
4	53.6	39.4	3.10
4	52.1	45.1	3.10
4	53.3	44.8	3.10

$\beta = 15°$: 4th July to 14 Nov 2015

PRIMARY DATA (Measured)			
P (kPa)	t_{in} (s)	t_{out} (s)	V (L)
4	38.6	32.6	3.07
4	38.3	35.2	3.04
4	39.0	32.2	3.02
4	39.3	36.8	3.02
4	39.3	31.0	3.03
4	37.1	41.2	3.09
4	36.5	56.5	3.00
4	38.1	61.8	3.10
4	38.2	55.0	3.05
4	38.0	54.6	3.01
4	38.7	42.2	3.24
4	36.8	58.9	3.18
4	37.9	47.9	3.20
4	38.8	49.1	3.33
4	36.8	52.2	3.25

$\beta = 25°$: 4th July to 14 Nov 2015

PRIMARY DATA (Measured)			
P (kPa)	t_{in} (s)	t_{out} (s)	V (L)
4	36.2	39.4	3.05
4	37.4	40.7	3.12
4	36.5	41.4	2.95
4	36.8	42.4	2.96
4	36.5	41.6	2.87
4	36.5	35.4	3.14
4	37.7	35.5	3.16
4	36.0	40.1	3.13
4	36.1	37.9	3.07
4	36.9	38.9	3.14
4	37.1	44.3	3.21
4	37.6	45.4	3.13
4	36.9	44.4	3.19
4	37.4	46.3	3.17
4	36.9	47.3	3.20

The data for each set along with that for the rig in Table 1 were substituted into Eqs (16) to (21) to obtain 9 equations which were then solved using Engineering Equation Solver (EES) software. The results were graphed as in Fig. 7.
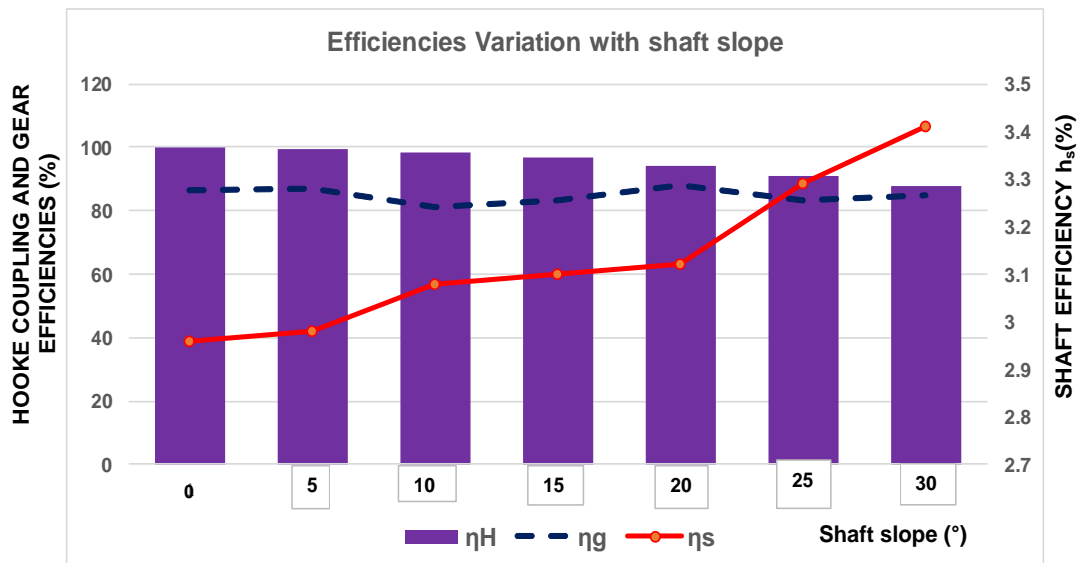

Fig. 7 Variation of mechanical efficiencies with Hooke joint shaft angle

4.4. Further experimentation for verification of results

Verification of the computed gear and shaft efficiencies was done by investigating times of travel between intended start-stop positions of the mechanism in the whole range of $0 \leq \emptyset \leq 180°$ for each value of angle β. Here, we illustrate the process by summarizing the procedure and analysis. We also sample results and show those for the angles $\beta = 10°$, $25°$ and $30°$.

4.4.1. Procedure of verification

The mechanism was run as intended for normal operation (i.e. allowing the drive masses to intermittently rotate the loaded shaft through 15° each step). Step-run times and discharge-fluid volumes were recorded as in section 4.3. The rotations were controlled by monitoring the position of the piston edge along the transparent part of the piston cylinder, and cutting off power supply to the solenoid valve when the piston reached a predetermined position. A tape measure with marked off computed piston positions had been affixed along the piston cylinder for the purpose. The 12 run times and volumes were then used to compute individual average step flow rates. This procedure was repeated 5 times on different days for each angle.

4.4.2. Analysis

A theoretical analysis for each step was done by balancing energy transfers and transformations around the hydraulic system of Fig. 5. The analysis used the flow discharges (ΔV) in section 4.4.1, vertical distances from the design geometry (x, y, $\overline{y}_b$, etc.), and values of efficiencies in Fig. 7. These were substituted in Eq. (22) below to obtain an equation for each step's run time. The equation was then solved using EES software for each step – with pressure and volume values being determined recursively from mechanism geometry and statics (for P_{static}), and cumulative outflow (for V_{rem}) at each step. These run times were compared to actual measurements to verify the efficiencies. The results were therefore, to be as much a check on the accuracy of the model as they were on the accuracy of bladder construction to specification.

In Figs. 1 and 3, the unsteady flow of a volume ΔV (liter) out of the bladder in a time t_{out} (s) to cause a step rotation from position $\emptyset_1$ to $\emptyset_2$ (Rad) and leave a volume V_{rem} (liter) in the bladder yields one of the relations in Eq. (22) when rig data is substituted into the bladder energy balance equation. All units of distances have in these equations been left in the measured form – i.e. mm. Pressure is, however, expressed in Pa.

For $0 < \emptyset < p/2$ (i.e. $0 < x < 0.5x_{max}$):

$$E_{g-out1} + \Delta E_f = E_{f-out} + E_{r-fout}$$

$$= 0.113\eta_g \Delta x - \frac{1.317\Delta \sin \varphi}{\eta_s \eta_{H\varphi_1,\varphi_2}} + 9.792 \left[(x+\overline{y})V_{rem}|_{\varphi_2} - (x+\overline{y})V_{rem}|_{\varphi_1} + \Delta V \overline{z}_{\Delta V} \right]$$

$$+ 0.001 \left[P_v V_{rem}|_{\varphi_1} - P_v V_{rem}|_{\varphi_2} \right] = 1.469\Delta V + \left[34.11 + 7.45 \left(\frac{t_{out}}{\Delta V} \right)^{0.25} \right] \frac{(\Delta V)^3}{t_{out}^2}$$

(22a)

And for $p/2 < \emptyset < p$ (i.e. $0.5x_{max} < x < x_{max}$):

$$E_{g-out2} + \Delta E_f = E_{f-out} + E_{r-fout}$$

$$= 0.113\eta_g \Delta x + 1.317\eta_g \eta_s \eta_{H\varphi_1,\varphi_2} \Delta \sin \varphi + 0.00979 \left[(x+\overline{y})V_{rem}|_{\varphi_2} - (x+\overline{y})V_{rem}|_{\varphi_1} + \Delta V \overline{z}_{\Delta V} \right]$$

$$+ 0.001 \left[P_v V_{rem}|_{\varphi_1} - P_v V_{rem}|_{\varphi_2} \right] = 1.469\Delta V + \left[34.11 + 7.45 \left(\frac{t_{out}}{\Delta V} \right)^{0.25} \right] \frac{(\Delta V)^3}{t_{out}^2}$$

(22b)

$$P_v = P_{static} + 0.001\rho_f g\overline{y}$$

(22c)

where $\overline{y}$ (mm) is distance of centroid of V_{rem} from piston and $\overline{z}_{\Delta V}$ (mm) is the height of the centroid of the removed volume ΔV above that of the centroid of fluid which remains in the bladder when the piston reaches BDC.

4.4.3. Verification

Fig. 8 gives sample results of the comparison. The first two figures typify the repetition of data acquisition for these experiments. The third one compares only average run times with theory. These actual averages were to be used in a subsequent project stage of design of the mechanism's control system.

5. Discussion

5.1. Efficiencies

In Fig. 7, the Hooke coupling efficiency is seen to gradually reduce from 100% at 0° shaft angle to 87.5% at 30°. This is the theoretical variation derived from geometry of the coupling. The analysis presupposed that friction between elements making the coupling was small and negligible. The spur gear-rack set efficiency appeared to vary slightly in the range of Hooke shaft angles considered. For the 99 valid result sets in the period, it averaged 84.8% with a 5.4% standard deviation. The mean of the averages for the 7 shaft angles was, however, more uniform at 84.8% with a standard deviation of 2.34%. According to Hindhede, et al. [12] and Rothbart [13], well lubricated commercial spur gearing loaded at capacity is known to have efficiencies of up to 98.5% per stage if in continuous operation. Here, motion is - by design function - intermittent. Secondly, the loading is minimal in comparison with capacity. For steel gears, a drastic fall of efficiency from 97% at loads below 30% of capacity is shown in [13]. The drop in efficiency in this work was thus, in line with established realities on loading. Thirdly, it was not feasible to sustain good lubrication during the test period because of intermittent exposures to weather elements necessitated by the development nature of the work. In summary, therefore, lower than normal gear-rack set efficiencies were obtained in the prototype but they could possibly be improved in a reengineered product for commercial development. One possibility is a change to use more corrosion resistant and lesser friction gear materials - such as some plastics described by Davis [14] and Avallone, et al. [15].

The shaft efficiencies (η_s), were very low. For the 99 valid result sets, they averaged 3.12% with a standard deviation of 0.16%. A closer look at the values - exposed by a separate large scale in Fig. 7, however, indicates an underlying variation with Hooke shaft angle β. It seems that even within its generally small value, the efficiency increases with the angle. In theory, inefficiencies are expected to arise partly from semi fixed effects of the splined coupling (between Hooke joint and shaft), rolling contact bearings and from variable effects of wind resistance/disturbance on the installation. Waldron couplings with involute teeth as used in the prototype are known to have transmission efficiencies of the order of that in normal spur gearing if shaft misalignment is minimal. Well housed pillow block bearings on the other hand should have about 99% a pair. In the installation, there was exposure of the inner bearing cages to the elements. This may have compromised bearing efficiencies in spite of attempts at anticorrosion treatment and lubrication. Misalignment between the Hooke joint and the shaft in the coupling, occasioned by numerous Hooke angle changes could also have contributed to lowering the splined coupling efficiency.

Wind exerts stochastic forces on the rotating mass and its support structure. Wind speeds during the experiments varied between 0 and 6.95 m/s from all directions. As far as the rotating mass is concerned, although acted on by drag and lift forces, rotation about an axis parallel and close to that of symmetry (e = 0.0136 m) minimized resistance and disturbance torques from the forces. However, the effect on the support structure remained and could have aggravated misalignment effects, already described. The positive learning element from this was that there could be some room for improvement of efficiencies by stiffening the support structure.

5.2. Verification of the derived efficiencies

In Fig. 8, intermittent run times obtained by computation using η_g and η_s values of Fig. 7 were compared with actual values. Computations used different Hooke coupling efficiencies for each step in line with equation (20a). In general, all results

showed varying differences between actual and theoretical times. First, this might be as expected because the modelling for efficiencies relied on potential energy terms only as the kinetic ones were relatively small. Moreover, as pointed out earlier, it ignored Hooke coupling friction. Close observation shows that the use of these theoretical efficiencies overestimated run times in the first 3 to 4 of 12 steps. This seems to suggest that actual efficiencies at $\emptyset$ angles less than 45° might be higher than the averaged values for a full 180° rotation. This could probably arise from at least two effects: the first is, shock loading at each beginning of run owing to sudden opening of the valve. This effect is more pronounced in earlier step runs because the distances retracted by the piston (Δx) are then smaller (e.g. 9.8 mm for 1st step against 14.1 mm for the 6th) due to the bladder geometry. The second is evident from Eq. (8). This equation suggests that the theoretical instantaneous efficiency of the Hooke coupling at low values of $\emptyset$ is higher than the average value for a full 180° rotation given by Eq. (20a) with $\emptyset_1 = 0$ and $\emptyset_2 = \pi$. Apart from a possible influence on the performance of the Waldron coupling (linking the Hooke joint to the rotating mass shaft) by the shock loading, it is still unclear whether the shaft efficiency η_s is significantly affected in these early steps.
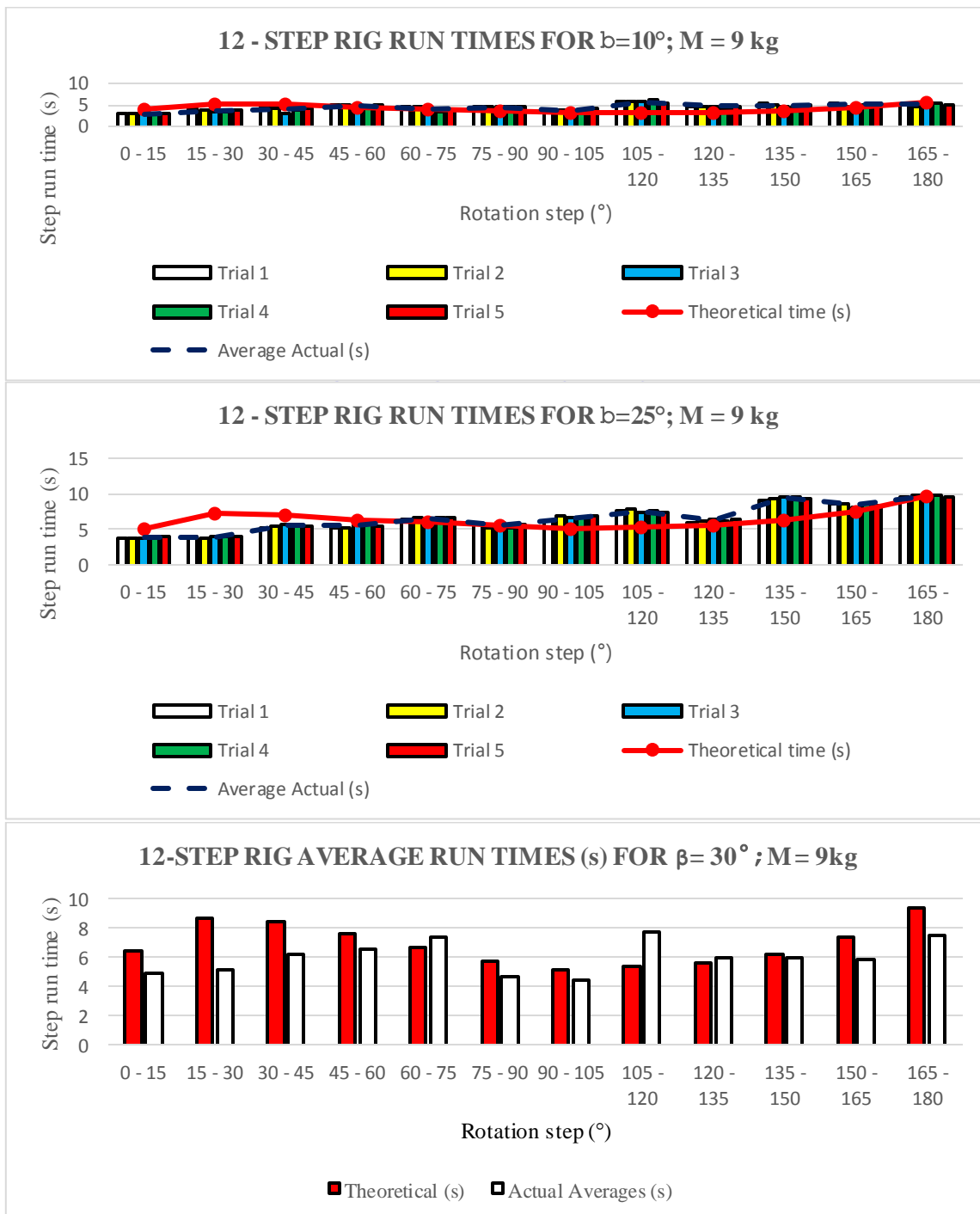

Fig. 8 Verifying efficiencies: theoretical compared with actual run times for β = 0°, 25° and 30°

There was closer agreement between theory and actuals in mid to end step runs except for the $105°$ to $120°$ step, where 'theory' this time grossly under estimated (by over 30% in most cases) run times for many angles β. The reason for this is still unclear but it could probably be due to inaccuracies in construction of the bladder and /or its protective covering in this part. This seems to be supported by evidence on volumes: whereas, the theoretical volume of the bladder part being emptied is 2.45 liter, summations of actual ΔV values in $180°$ averaged 3.1 liter - indicating a possible minimum of 8.16% error in dimensions of the part. For the 7 Hooke shaft angles, in the $135° - 150°$ step, the 32% under estimate when $\beta = 25°$ was an exception rather than the rule.

6. Conclusion

A new hydro-mechanical mechanism had been designed and constructed. It has now been theoretically modelled for energy transfers and mechanically tested. Experimental results on application in a prototype solar tracker indicated that while the mechanism's design concept works well, improvements on how it uses energy could still be made. As expected, the modelling showed that the higher the Hooke shaft angle, the lower the joint efficiency. The gear - rack set efficiency was reasonably high in the 80-90% range for all Hooke shaft angles tested. With a change in gear materials from steel to a plastic (e.g. Acetal, Nylon 6, etc.), literature seems to suggest that it might be possible to improve this value to the 90s range. The rotating mass shaft efficiency - as influenced by the Waldron coupling, the support bearings and frame - perhaps gives the biggest potential for improvement. Current prototype shaft efficiencies are below 4% for all angles. Improved frame stiffness - e.g. by construction from steel sections as opposed to current aluminum - might help reduce lateral vibrations of the structure in windy conditions, and hence, reduce tendency to misalignment between rotating mass shaft and Hooke joint output shaft. This would improve the efficiency significantly.

To conclude, the main contributions of this work were the following:

(1) Identification and estimation of key design variables to enable future improvements in a commercial development of a product utilizing the new mechanism. The most critical pairing element was the shaft-Hooke subsystem. Redesign of this could consider three actions:

    i.   Strengthen and stiffen support structure to prevent bearings misalignments caused by wind loads

    ii.   Change the Waldron coupling to a rigid type to connect the rotating mass shaft to the Hooke coupling since experimental work that necessitated use of the Waldron type will not be done by users in the field.

    iii.   Ensure proper shielding of the shaft bearings against the elements - since the variation of tilt angle by the user will not be necessary in the field.

(2) In the case of solar tracking, a clear indication of the magnitudes of intermittent step run times for use in the next stage of tracker control system design.

(3) Again for solar tracking, a clear indication of the pressure head necessary to run the tracker irrespective of its source. This is important because as mentioned in [1] and [2], one of the product specifications was able to run without any source of electrical power.

    i.   These three objectives were achieved and consequently, the project was able to progress in successive stages.

References

[1] K. E. Kanyarusoke and J. Gryzagoridis, A hydraulic mechanism, solar tracker, South Africa Patent, P72557Z, January 2016.

[2] K. E. Kanyarusoke and J. Gryzagoridis, "The new hydro-mechanical solar tracker: performance testing with a PV panel," Proc. International Conf. Domestic Use of Energy, March 2016, pp. 178-185.

[3] N. Jain, "Reduction in parasitic load in a solar thermal power plant to improve its efficiency," International Journal of Scientific Research and Reviews, vol. 2, no. 1, pp. 24-29, Januany 2013.

[4] Y. A. Çéngel and M. A. Boles, Thermodynamics: an engineering approach, 8th ed. SI units. New York: Mc Graw Hill, 2015.

[5] H. H. Mabie and C. F. Reinholtz, Mechanisms and dynamics of machinery, London: Wiley and Sons, 1987.

[6] D. S. Kumar, Automobile engineering, New Delhi: S. K. Kataria & Sons, 2015.

[7] A. A. Alugongo, "Parametric excitation and wavelet transform analysis of a ground vehicle propeller shaft," Journal of Vibrations and Control, vol. 20, no. 2, pp. 280-289, Februay 2014.

[8] I. S. Fischer and R. N. Paul, "Kinematic displacement analysis of a double-cardan-joint driveline," Journal of Mechanical Design, vol. 113, no. 3, pp. 263-271, September 1991.

[9] Y. A. Çéngel and J. M. Cimbala, Fluid Mechanics fundamentals and applications, 3rd ed. SI units. New York: McGraw Hill, 2014.

[10] J. F. Douglas, J. M. Gasiorek, J. A. Swaffield, and L. B. Jack, Fluid mechanics, 6th ed.. London: Pearson, 2011.

[11] K. E. Kanyarusoke, J. Gryzagoridis, and G. Oliver, "Validation of TRNSYS modelling for a fixed slope photovoltaic panel," Turkish Journal of Electrical Engineering and Computer Science, vol. 24, no. 6, pp. 4763-4772, December 2016.

[12] U. Hindhede, J. R. Zimmerman, R. B. Hopkins, R. J. Erisman, W. C. Hull, and J. D. Lang, Machine design fundamentals, New York: Wiley, 1993.

[13] H. A. Rothbart, Mechanical design handbook, New York: Mc Graw Hill, 1996.

[14] J. R. Davis, Gear Materials, Properties, and manufacture, Ohio, USA: ASM International, 2005.

[15] E. A. Avallone, T. Baumeister III, and A. M. Sadech, Mark's Standard handbook for mechanical engineers, 11th ed. New York: Mc Graw Hill, 2007.